agreement may be in part fortuitous, it is gratifying that a series of experiments on intracomplex electron transfer as a function of driving force and a series on intermolecular electron transfer as a function of temperature and ionic strength lead to the same conclusion.

Heme Protein Reorganization Energies. Our reorganization energies for cytochrome *c* and cytochrome b_5 can be compared with those for electron transfer in a number of heme proteins given in Table IV. The reorganization energies have been calculated from the dependence of the electron-transfer rate constants on temperature (T) or on the driving force (E) of the reaction. Both protein–protein and protein–small molecule reagent pairs have been investigated; reactions studied include those with intramolecular, intracomplex, and bimolecular electron transfer. The reorganization energies are between 0.8 and 2 eV. Our values for cytochromes *c* and cytochrome b_5 are in the range of other heme protein electron-transfer reactions, indicating that comparisons of intramolecular and intermolecular electron transfer as well as calculations via the dependence of the rate constants on temperature or energy all give similar values for the reorganization energy.

Acknowledgment. We thank the National Institutes of Health (Grant DK 38826 to D.W.D.) and the Medical Research Council of Canada (Grant MT-7182 to A.G.M) for support of this work. D.W.D. thanks the National Science Foundation for a Career Advancement Award (NSF CHE 8707447). The Varian VXR400 NMR spectrometer at G.S.U. was purchased with funds from the NSF Instrumentation Program (CHEM-809599).

Registry No. Cytochrome b_5, 9035-39-6.

(37) Sutin, N.; Creutz, C.; Linck, R. G. In *Inorganic Reactions and Methods*; Zuckerman, J. J., Ed.; VCH Publishers: Deerfield Beach, FL, 1986; Vol. 15, p 3.

Periodic Trends in Charge Distribution for Transition-Metal Complexes Containing Catecholate and Semiquinone Ligands. Synthetic, Physical, and Stereodynamic Properties of the Tris(3,5-di-*tert*-butylquinone) Complexes of Ruthenium and Osmium

Samaresh Bhattacharya, Steven R. Boone, Glenn A. Fox, and Cortlandt G. Pierpont*

Contribution from the Department of Chemistry and Biochemistry, University of Colorado, Boulder, Colorado 80309. *Received March 27, 1989*

Abstract: Tris(3,5-di-*tert*-butylbenzoquinone) complexes of Ru and Os have been synthesized in the interest of investigating periodic trends in charge distribution for tris(quinone) complexes of second- and third-row transition metals. Infrared spectra of the two complexes are similar but differ from spectra obtained on related semiquinone [$Fe(DBSQ)_3$] and catecholate [$Re(DBCat)_3$] complexes. Both complexes undergo two oxidation and two reduction reactions at similar potentials. Crystallographic characterization on the cis and trans isomers of $Ru(DBQ)_3$ and on *trans*-$Os(DBQ)_3$ at −60 °C shows short M–O bond lengths, typical of complexes containing high oxidation state forms of Ru and Os. Ligand C–O bond lengths are found to be intermediate between semiquinone and catecholate values, with lengths that are more semiquinone-like for $Ru(DBQ)_3$ and more catecholate-like for $Os(DBQ)_3$. This subtle difference in charge distribution between the second- and third-row metals appears to contribute to marked differences in the stereodynamic properties of the two complexes. Both are diamagnetic and show sharp NMR spectra at room temperature. Eight *tert*-butyl and eight ring proton resonances are observed for $Ru(DBQ)_3$ at room temperature, indicating the presence of stereochemically rigid cis and trans isomers. Two *tert*-butyl and two ring proton resonances are observed for $Os(DBQ)_3$ at room temperature. At −85 °C eight *tert*-butyl and eight ring proton resonances appear as molecular rearrangement rates decrease on the NMR time scale. Analysis of the temperature dependence of the spectrum of $Os(DBQ)_3$ has indicated racemization by a trigonal twist mechanism at lower temperatures, with structural isomerization and racemization by a rhombic twist mechanism at higher temperatures.

Localized quinone and metal electronic levels in complexes containing semiquinonate and catecholate ligands are close in energy. The resulting ambiguity in charge distribution has become a unique property of complexes containing chelated quinone ligands. Studies have shown that, for a particular ligand, effects that change the order of metal orbital energy relative to the energy of the quinone π orbital can result in a change in the electron distribution within the complex. The most widely studied quinone ligand in this regard is 3,5-di-*tert*-butylbenzoquinone (DBBQ), coordinated in its reduced catecholate (DBCat) and semiquinonate (DBSQ) forms. Charge distribution in the $L_2Cu^{II}(DBCat)/L_2Cu^{I}(DBSQ)$ unit has been shown to depend upon the donor nature of the counter ligand L.[1] Hard nitrogen donors favor Cu(II); soft phosphine donors result in the Cu(I) charge distribution (Chart I). A change in the net charge of a complex may result in a change in electron distribution. This property has been studied for the $Mn^{II}(DBSQ)_2/Mn^{III}(DBCat)_2^-$ and $V^{III}(DBSQ)_3/V^{V}(DBCat)_3^-$ couples where, ironically, reduction of the complex leads to oxidation of the metal.[2,3] Thermal changes

Chart I

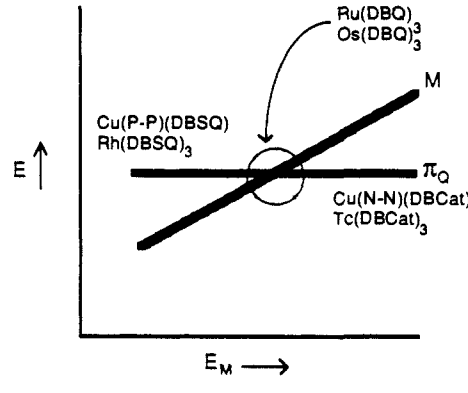

(I)

(1) Buchanan, R. M.; Wilson-Blumenberg, C.; Trapp, C.; Larsen, S. K.; Greene, D. L.; Pierpont, C. G. *Inorg. Chem.* **1986**, *25*, 3070.

0002-7863/90/1512-1088$02.50/0

in charge distribution have been studied for $Co^{II}(bpy)(DBSQ)_2/Co^{III}(bpy)(DBSQ)(DBCat)$ and $Mn^{II}(py)_2(DBSQ)_2/Mn^{IV}(py)_2(DBCat)_2$.[4,5] These features of variable-charge distribution may be described in terms of the relative orbital energies of the quinone (π_Q) and metal (M) shown in Chart I. To the right of the crossing point, metal orbital energy is higher than the energy of π_Q and the quinone ligand would be in the reduced catecholate form. $Cu^{II}(N-N)(DBCat)$ illustrates this charge distribution. To the left of the crossing point, π_Q is higher in energy than M; the metal would be in the reduced state, and $Cu^{I}(P-P)(DBSQ)$ is an example of this condition.

Perhaps the most straightforward factor influencing charge distribution in the neutral $M(DBQ)_2$ and $M(DBQ)_3$ complexes is the periodic dependence of metal orbital energy. Within a congeneric group of metals, complexes containing the 3d metals of the first transition series all have either the $M^{II}(DBSQ)_2$ (M = Mn, Co, Ni, Cu) or $M^{III}(DBSQ)_3$ (M = V, Cr, Fe) charge distributions.[6-11] Complexes of the Cr, Mo, W and Mn, Tc, Re triads illustrate the periodic effect with the shift to higher metal oxidation states and reduced catecholate ligands for the $M^{VI}(DBCat)_3$ (M = Mo, W, Tc, Re) series as metal orbital energy increases for the 4d and 5d members of the groups.[12-15] The periodic effect of increased orbital stability across a transition series is becoming apparent. The $Pd^{II}(DBSQ)_2$ units of $Pd_2[Pd(DBSQ)_2]_2$ have more reduced metal ions than other related complexes of the second transition series, and in the absence of the stabilizing effect of the organometallic bonding by the additional palladium atoms, the $Pd(DBSQ)_2$ unit is subject to disproportionation to Pd metal and DBBQ.[16] Recent characterization of the rhodium complex $Rh^{III}(DBSQ)_3$ further illustrates the change in charge distribution that occurs across the second transition series as the 4d level fills.[17] This result, with the high oxidation state of technetium in $Tc^{VI}(DBCat)_3$,[14] has stimulated interest in the charge distribution and physical properties of the ruthenium analogue $Ru(DBQ)_3$. This complex would lie close to the crossing point for metal and quinone orbital energies in Chart I, and in this case there is potential for low-energy intramolecular charge transfer between the metal and the chelated quinone ligands. In an earlier study on the osmium analogue there was the appearance of mixed-charge ligands as a possible consequence of this electronic structure.[18] Other recent studies on $Ru(N-N)(DBQ)_2$ complexes have shown intense low-energy charge-transfer bands in the near-infrared and features that suggest a charge for the ligands that is intermediate between those of catecholate and semiquinone.[19,20] This ambiguity in charge distribution has been attributed to mixing of metal and quinone electronic levels that are close in energy. In this report we describe the synthesis of $Ru(DBQ)_3$, the results of characterization on the complex, the results of additional characterization on $Os(DBQ)_3$, and the unusual stereodynamic properties of $Os(DBQ)_3$.

Table I. Crystal Data for *cis*-$Ru(DBQ)_3 \cdot C_2H_5OH$, *trans*-$Ru(DBQ)_3$, and *trans*-$Os(DBQ)_3$

	cis-$Ru(DBQ)_3 \cdot C_2H_5OH$	*trans*-$Ru(DBQ)_3$	*trans*-$Os(DBQ)_3$
formula	$RuC_{44}H_{66}O_7$	$RuC_{42}H_{60}O_6$	$OsC_{42}H_{60}O_6$
mol wt	804.03	762.00	851.13
space group	$P\bar{1}$	$P2_1/c$	$P2_1/c$
a, Å	10.210 (3)	19.357 (9)	19.278 (7)
b, Å	11.812 (4)	10.579 (6)	10.487 (6)
c, Å	19.052 (6)	20.669 (11)	20.689 (9)
α, deg	77.78 (3)	90.00	90.00
β, deg	81.23 (2)	97.73 (4)	98.11 (3)
γ, deg	85.05 (3)	90.00	90.00
V, Å^3	2216 (1)	4194 (4)	4141 (3)
Z	2	4	4
T, K	298	298	213
λ, Å		0.71073 (Mo Kα)	
ρ_{meas}, g/cm^3	1.20 (2)	1.18 (2)	1.38 (2)
ρ_{calc}, g/cm^3	1.20	1.21	1.37
μ, mm^{-1}	0.39	0.41	3.12
R, R_w (obsd data)	0.056, 0.076	0.058, 0.076	0.047, 0.061

Experimental Section

Synthesis of $Ru(DBQ)_3$. 3,5-Di-*tert*-butylcatechol (0.70 g, 3.15 mmol) and KOH (0.36 g, 6.43 mmol) were added to a solution of $RuCl_3 \cdot 3H_2O$ (0.20 g, 0.76 mmol) dissolved in 30 mL of methanol. The solution was stirred for 24 h at room temperature. Solvent was removed under reduced pressure to give a dark blue solid. The solid was dissolved in benzene, and the solution was filtered. The filtrate was passed through an alumina column with benzene as the eluant. A purple band containing $Ru(DBQ)_3$ was collected, and, upon slow evaporation of the solvent, dark purple crystals (0.27 g) were obtained in 46% yield. Crystals suitable for crystallographic investigation were grown by slow evaporation of a 1:1 acetone–ethanol solution.

Synthesis of $Os(DBQ)_3$. A sample of $Os(DBQ)_3$ was prepared by the reaction between OsO_4 and 3,5-di-*tert*-butylcatechol according to the procedure described earlier by Griffith.[18] Crystals of the complex suitable for crystallographic study were grown by slow evaporation of a chloroform solution.

Physical Measurements. Infrared spectra were recorded on an IBM IR/30 FTIR spectrometer with samples prepared as KBr pellets. UV/vis spectra were recorded on a HP 8451A diode array spectrophotometer, and UV/vis/near-infrared spectra were recorded on a Perkin-Elmer Lambda 9 spectrophotometer. A Varian E-109 spectrometer was used for EPR spectra, with DPPH ($g = 2.0037$) used as the g-value standard. ^1H NMR spectra were recorded on a Varian VXR 300S spectrometer. NMR spectrum simulations were carried out with the programs ADNMR and ADPLOT. Cyclic voltammograms were obtained with a BAS-100 electrochemical analyzer in CH_2Cl_2 solutions. A platinum disk working electrode and a platinum wire counter electrode were used. The reference electrode was based on the Ag/Ag^+ couple and consisted of a CH_3CN solution of $AgPF_6$ in contact with a silver wire placed in glass tubing with a Vycor frit at one end to allow ion transport. Tetrabutylammonium hexafluorophosphate (TBHP) was used as the supporting electrolyte, and the ferrocene/ferrocenium couple was used as an internal standard. The Fc/Fc^+ couple was found to occur at 0.14 V in this experimental arrangement.

Crystallographic Structure Determination on *cis*-$Ru(DBQ)_3 \cdot C_2H_5OH$. Crystals of *cis*-$Ru(DBQ)_3$ form as rhombic blocks. A crystal of the complex was mounted and aligned on a Nicolet P3/F automated diffractometer. Axial photographs indicated triclinic symmetry, and the centered settings of 25 reflections gave the unit cell dimensions given in Table I. Parameters and procedures used for data collection, structure determination, and refinement are given in tables included with the supplementary material. The location of the Ru atom was determined

(2) Larsen, S. K.; Pierpont, C. G.; DiMunno, G.; Dolcetti, G. *Inorg. Chem.* **1986**, *25*, 4828.
(3) Cass, M. E.; Gordon, N. R.; Pierpont, C. G. *Inorg. Chem.* **1986**, *25*, 3962.
(4) Buchanan, R. M.; Pierpont, C. G. *J. Am. Chem. Soc.* **1980**, *102*, 4951.
(5) Lynch, M. W.; Hendrickson, D. N.; Fitzgerald, B. J.; Pierpont, C. G. *J. Am. Chem. Soc.* **1984**, *106*, 2041.
(6) Buchanan, R. M.; Pierpont, C. G. *Inorg. Chem.* **1979**, *18*, 3439.
(7) Kahn, O.; Prins, R.; Reedijk, J.; Thompson, J. S. *Inorg. Chem.* **1987**, *26*, 3557.
(8) We recently noted an exception to this trend in charge distribution. The $Fe_4(DBSQ)_4(DBCat)_4$ tetramer, which is isostructural with $M_4(DBSQ)_8$ (M = Mn, Co, Ni) contains mixed-charge semiquinone and catecholate ligands.[9]
(9) Boone, S. R.; Purser, G. H.; Chang, H.-R.; Lowery, M. D.; Hendrickson, D. N.; Pierpont, C. G. *J. Am. Chem. Soc.* **1989**, *111*, 2292.
(10) Cass, M. E.; Greene, D. L.; Buchanan, R. M.; Pierpont, C. G. *J. Am. Chem. Soc.* **1983**, *105*, 2680.
(11) (a) Sofen, S. R.; Ware, D. C.; Cooper, S. R.; Raymond, K. N. *Inorg. Chem.* **1979**, *18*, 234. (b) Buchanan, R. M.; Kessel, S. L.; Downs, H. H.; Pierpont, C. G.; Hendrickson, D. N. *J. Am. Chem. Soc.* **1978**, *100*, 7894.
(12) Cass, M. E.; Pierpont, C. G. *Inorg. Chem.* **1986**, *25*, 122.
(13) Beshouri, S. M.; Rothwell, I. P. *Inorg. Chem.* **1986**, *25*, 1962.
(14) deLearie, L. A.; Haltiwanger, R. C.; Pierpont, C. G. *J. Am. Chem. Soc.* **1989**, *111*, 4324.
(15) deLearie, L. A.; Haltiwanger, R. C.; Pierpont, C. G. *Inorg. Chem.* **1987**, *26*, 817.
(16) Fox, G. A.; Pierpont, C. G. *J. Chem. Soc., Chem. Commun.* **1988**, 806.
(17) Dodsworth, E. S.; Morgans, H. J.; Lever, A. B. P. XXVI International Conference on Coordination Chemistry, Porto, Portugal, 1988; Abstract A94.
(18) (a) Hursthouse, M. B.; Fram, T.; New, L.; Griffith, W. P.; Nielson, A. J. *Transition Met. Chem. (Weinheim, Ger.)* **1978**, *3*, 255. (b) Nielson, A. J.; Griffith, W. P. *J. Chem. Soc., Dalton Trans.* **1978**, 1501.
(19) Haga, M.; Dodsworth, E. S.; Lever, A. B. P.; Boone, S. R.; Pierpont, C. G. *J. Am. Chem. Soc.* **1986**, *108*, 7413.
(20) Lever, A. B. P.; Auburn, P. R.; Dodsworth, E. S.; Haga, M.; Liu, W.; Melnik, M.; Nevin, W. A. *J. Am. Chem. Soc.* **1988**, *110*, 8076.

Table II. Atomic Coordinates (×10⁴) and Equivalent Isotropic Displacement Parameters (Å² × 10⁴) for *cis*-Ru($O_2C_{14}H_{20}$)$_3$

atom	x/a	y/b	z/c	U (eq)[a]
Ru	2414 (1)	2501 (1)	1380 (1)	299 (2)
O1	3878 (3)	3322 (3)	716 (2)	349 (12)
O2	2418 (3)	1802 (3)	518 (2)	296 (11)
O3	3736 (3)	1395 (3)	1831 (2)	353 (12)
O4	1202 (3)	1476 (3)	2093 (2)	296 (11)
O5	2307 (3)	3436 (3)	2137 (2)	379 (13)
O6	782 (3)	3454 (3)	1169 (2)	346 (12)
C1	4287 (5)	2870 (4)	139 (2)	279 (16)
C2	3415 (5)	2069 (4)	15 (2)	261 (15)
C3	3647 (5)	1637 (4)	−650 (2)	281 (16)
C4	4810 (5)	1954 (4)	−1088 (3)	303 (16)
C5	5739 (5)	2686 (4)	−944 (3)	308 (16)
C6	5454 (5)	3167 (4)	−331 (2)	299 (16)
C7	2660 (5)	872 (5)	−824 (3)	344 (18)
C8	3160 (6)	468 (6)	−1535 (3)	489 (22)
C9	2461 (7)	−220 (5)	−228 (3)	540 (24)
C10	1325 (6)	1569 (6)	−891 (3)	547 (25)
C11	6986 (5)	2980 (5)	−1496 (3)	375 (18)
C12	8001 (5)	3514 (6)	−1188 (3)	465 (21)
C13	7624 (6)	1862 (6)	−1740 (3)	525 (23)
C14	6549 (6)	3827 (6)	−2165 (3)	484 (22)
C15	3222 (5)	729 (5)	2446 (3)	335 (18)
C16	1818 (5)	771 (4)	2589 (3)	286 (16)
C17	1165 (5)	85 (4)	3221 (3)	281 (16)
C18	1978 (5)	−631 (5)	3670 (3)	325 (17)
C19	3388 (5)	−689 (5)	3535 (3)	339 (18)
C20	3998 (5)	−12 (5)	2918 (3)	362 (18)
C21	−342 (5)	161 (5)	3404 (3)	322 (17)
C22	−820 (5)	1398 (5)	3490 (3)	470 (21)
C23	−831 (5)	−663 (5)	4119 (3)	423 (20)
C24	−962 (5)	−164 (6)	2797 (3)	475 (22)
C25	4152 (5)	−1510 (5)	4082 (3)	409 (19)
C26	3686 (7)	−1304 (7)	4850 (3)	644 (28)
C27	5624 (6)	−1324 (7)	3928 (3)	624 (27)
C28	3922 (7)	−2765 (6)	4069 (4)	656 (28)
C29	1055 (5)	3851 (4)	2269 (3)	309 (17)
C30	213 (5)	3828 (4)	1755 (3)	326 (17)
C31	−1148 (5)	4229 (5)	1857 (3)	370 (18)
C32	−1536 (6)	4679 (5)	2477 (3)	429 (20)
C33	−674 (6)	4753 (5)	2987 (3)	402 (19)
C34	605 (6)	4335 (5)	2887 (3)	415 (20)
C35	−2109 (6)	4106 (5)	1336 (3)	447 (21)
C36	−1645 (7)	4826 (6)	585 (3)	617 (27)
C37	−2157 (7)	2857 (6)	1301 (4)	618 (27)
C38	−3517 (6)	4574 (7)	1568 (4)	663 (30)
C39	−1238 (7)	5273 (6)	3650 (4)	570 (26)
C40	−124 (36)	5880 (29)	3878 (20)	1075 (151)
C41	−2467 (38)	5967 (44)	3614 (18)	1958 (252)
C42	−2423 (41)	4649 (32)	4021 (13)	1841 (191)
C40A	−180 (38)	5449 (46)	4090 (22)	1722 (266)
C41A	−1852 (32)	6503 (17)	3343 (12)	1063 (130)
C42A	−1514 (39)	4243 (22)	4317 (11)	1274 (172)
O60	2579 (6)	2182 (5)	4187 (3)	809 (15)
O61	4223 (9)	4041 (8)	3819 (4)	1392 (28)
C62	3796 (17)	2848 (14)	3612 (8)	1566 (52)
C63	3137 (15)	3523 (14)	4270 (8)	1564 (50)
C64	5129 (22)	2680 (19)	3378 (12)	2388 (89)

[a] Equivalent isotropic U defined as one-third of the trace of the orthogonalized U_{ij} tensor.

from a three-dimensional Patterson map, and the phases derived from the refinement of the metal atom were used to locate the non-hydrogen atoms of the structure. An ethanol solvate molecule was located on final difference Fourier maps. The oxygen and methylene carbon atoms of the solvent molecule were found to be disordered between two positions and were refined with half-occupancy factors at the two locations. Additionally, one *tert*-butyl group was found to suffer from 2-fold disorder and was refined with half-occupancies for the methyl carbon atoms. Final cycles of least-squares refinement converged with discrepancy indices of $R = 0.056$ and $R_w = 0.077$. Final positional and derived isotropic thermal parameters for all non-hydrogen atoms are listed in Table II. Tables containing anisotropic thermal parameters and hydrogen atom locations with thermal parameters are available as supplementary material.

Crystallographic Structure Determination on *trans*-Ru(DBQ)$_3$. Crystals of *trans*-Ru(DBQ)$_3$ form as small, thin plates. Axial photographs indicated monoclinic symmetry, and the centered settings of 23 reflections gave the unit cell dimensions given in Table I. The location of the Ru atom was determined from a three-dimensional Patterson map, and the phases derived from the refinement of the metal atom were used to locate all non-hydrogen atoms of the structure. Final cycles of least-squares refinement converged with discrepancy indices of $R = 0.058$ and $R_w = 0.076$. Final positional and derived isotropic thermal parameters for all non-hydrogen atoms are listed in Table III. Tables containing anisotropic thermal parameters and hydrogen atom locations with thermal parameters are available as supplementary material.

Table III. Atomic Coordinates (×10⁴) and Equivalent Isotropic Displacement Parameters (Å² × 10³) for *trans*-Ru($C_{14}H_{20}O_2$)$_3$

atom	x/a	y/b	z/c	U (eq)[a]
Ru	1815 (1)	2636 (1)	5706 (1)	41 (1)
O1	1543 (5)	1606 (10)	6441 (5)	49 (4)
O2	789 (4)	2541 (12)	5462 (4)	47 (4)
O3	1816 (5)	4326 (10)	6114 (5)	48 (4)
O4	2815 (5)	2779 (11)	5995 (5)	50 (4)
O5	2036 (5)	1128 (11)	5221 (5)	56 (5)
O6	1991 (5)	3507 (10)	4917 (5)	41 (4)
C1	877 (8)	1360 (15)	6404 (7)	42 (6)
C2	448 (9)	1946 (14)	5856 (7)	40 (6)
C3	−283 (8)	1737 (14)	5770 (7)	42 (6)
C4	−541 (8)	1034 (15)	6225 (8)	54 (7)
C5	−117 (9)	500 (16)	6796 (7)	55 (7)
C6	585 (7)	669 (15)	6860 (7)	48 (6)
C7	−741 (7)	2310 (17)	5168 (7)	51 (6)
C8	−559 (9)	1691 (17)	4559 (7)	74 (8)
C9	−1518 (8)	2080 (15)	5209 (8)	72 (8)
C10	−617 (8)	3748 (15)	5134 (9)	66 (8)
C11	−526 (10)	−166 (20)	7272 (9)	77 (9)
C12	−35 (11)	−642 (23)	7860 (10)	141 (13)
C13	−1033 (11)	698 (26)	7535 (11)	150 (16)
C14	−913 (11)	−1313 (22)	6935 (10)	138 (13)
C15	2428 (8)	4821 (17)	6137 (7)	46 (7)
C16	3008 (8)	3977 (18)	6099 (8)	53 (7)
C17	3696 (7)	4461 (17)	6143 (7)	44 (6)
C18	3768 (8)	5727 (19)	6259 (8)	58 (8)
C19	3203 (10)	6619 (18)	6290 (9)	60 (8)
C20	2543 (9)	6105 (18)	6258 (8)	55 (7)
C21	4292 (8)	3573 (22)	6095 (11)	79 (9)
C22	4242 (9)	2872 (21)	5466 (10)	110 (11)
C23	4994 (9)	4254 (21)	6186 (11)	123 (12)
C24	4328 (9)	2535 (20)	6642 (9)	97 (9)
C25	3404 (12)	8035 (20)	6357 (10)	74 (9)
C26	2747 (11)	8802 (18)	6476 (11)	99 (11)
C27	3946 (11)	8224 (17)	6967 (8)	80 (9)
C28	3691 (11)	8486 (21)	5767 (9)	110 (11)
C29	2388 (8)	1451 (16)	4767 (8)	46 (7)
C30	2362 (8)	2785 (17)	4558 (7)	51 (7)
C31	2679 (8)	3162 (17)	4022 (8)	51 (7)
C32	3038 (8)	2273 (20)	3730 (7)	64 (8)
C33	3106 (9)	949 (17)	3914 (9)	56 (7)
C34	2727 (8)	579 (17)	4423 (8)	51 (7)
C35	2660 (9)	4519 (17)	3813 (8)	56 (7)
C36	1886 (8)	4878 (17)	3578 (9)	78 (8)
C37	2924 (10)	5395 (17)	4363 (10)	94 (10)
C38	3049 (11)	4771 (17)	3222 (9)	94 (10)
C39	3527 (11)	98 (23)	3552 (11)	86 (10)
C40	3513 (18)	−1164 (24)	3722 (14)	258 (27)
C41	3296 (18)	220 (25)	2836 (11)	201 (22)
C42	4266 (13)	515 (25)	3614 (18)	229 (27)

[a] Equivalent isotropic U defined as one-third of the trace of the orthogonalized U_{ij} tensor.

Crystallographic Structure Determination on *trans*-Os(DBQ)$_3$ at −60 °C. The room-temperature structure of *trans*-Os(DBQ)$_3$ was reported earlier by Hursthouse and Griffith.[18a] A crystal of the complex was mounted and aligned on the diffractometer and cooled to −60 °C. The centered settings of 25 reflections were used to obtain the unit cell dimensions given in Table I. These dimensions and other information on the unit cell agree with values reported earlier and are quite similar to values obtained for the Ru analogue. A data set was collected at −60 °C, and a low-temperature structure determination was carried out with these data and the atom positions obtained from the structure determination on *trans*-Ru(DBQ)$_3$. Final cycles of least-squares refinement converged with discrepancy indices of $R = 0.047$ and $R_w = 0.061$. Final positional and derived isotropic thermal parameters are given in Table IV. Tables containing information on procedures followed in the structure deter-

Table IV. Atomic Coordinates ($\times 10^4$) and Equivalent Isotropic Displacement Parameters ($Å^2 \times 10^3$) for $Os(C_{14}H_{20}O_2)_3$

atom	*x/a*	*y/b*	*z/c*	*U*[a]
Os	1818 (1)	2621 (1)	5698 (1)	31 (1)
O1	1552 (4)	1577 (7)	6424 (3)	35 (3)
O2	803 (4)	2546 (6)	5465 (3)	36 (2)
O3	1815 (4)	4308 (7)	6109 (3)	38 (3)
O4	2820 (4)	2800 (7)	5999 (3)	41 (3)
O5	2034 (4)	1124 (6)	5202 (3)	36 (3)
O6	2005 (4)	3470 (7)	4904 (3)	37 (3)
C1	877 (5)	1362 (9)	6400 (5)	31 (4)
C2	451 (5)	1888 (9)	5855 (5)	27 (3)
C3	−287 (5)	1739 (9)	5761 (5)	30 (4)
C4	−546 (5)	1010 (9)	6222 (5)	38 (4)
C5	−129 (6)	468 (10)	6778 (5)	40 (4)
C6	582 (6)	623 (9)	6855 (5)	36 (4)
C7	−755 (6)	2336 (9)	5176 (5)	34 (4)
C8	−581 (7)	1686 (12)	4548 (5)	53 (5)
C9	−628 (6)	3752 (10)	5147 (7)	57 (5)
C10	−1536 (5)	2110 (11)	5209 (6)	46 (4)
C11	−505 (7)	−271 (16)	7263 (7)	73 (6)
C12	−1029 (8)	637 (19)	7523 (8)	118 (10)
C13	−892 (9)	−1413 (15)	6918 (8)	108 (8)
C14	12 (8)	−777 (19)	7833 (7)	120 (9)
C15	2439 (6)	4844 (10)	6151 (5)	40 (4)
C16	3001 (5)	4039 (11)	6086 (5)	40 (4)
C17	3698 (6)	4482 (11)	6152 (5)	40 (4)
C18	3793 (6)	5770 (11)	6245 (6)	49 (5)
C19	3225 (6)	6651 (11)	6301 (6)	45 (5)
C20	2558 (6)	6164 (11)	6259 (6)	45 (4)
C21	4321 (6)	3588 (12)	6104 (6)	51 (5)
C22	4349 (7)	2574 (12)	6653 (7)	65 (5)
C23	4239 (7)	2903 (14)	5454 (7)	73 (6)
C24	5025 (7)	4288 (15)	6206 (9)	98 (8)
C25	3402 (7)	8082 (13)	6382 (6)	55 (5)
C26	3944 (7)	8297 (13)	6968 (6)	66 (5)
C27	2736 (8)	8847 (12)	6478 (8)	86 (7)
C28	3669 (8)	8531 (13)	5770 (6)	76 (6)
C29	2403 (6)	1421 (9)	4724 (5)	35 (4)
C30	2375 (5)	2734 (9)	4544 (5)	36 (4)
C31	2697 (5)	3175 (11)	4013 (5)	38 (4)
C32	3047 (6)	2245 (11)	3710 (6)	46 (4)
C33	3102 (6)	951 (10)	3884 (6)	40 (4)
C34	2758 (6)	562 (10)	4381 (6)	43 (4)
C35	2655 (6)	4563 (11)	3798 (6)	44 (4)
C36	1879 (7)	4895 (12)	3596 (6)	63 (5)
C37	2944 (7)	5435 (11)	4367 (6)	59 (5)
C38	3036 (8)	4809 (13)	3208 (7)	70 (6)
C39	3523 (8)	84 (12)	3518 (8)	67 (6)
C40	3511 (13)	−1274 (14)	3733 (10)	174 (14)
C41	3311 (16)	227 (20)	2814 (10)	180 (16)
C42	4286 (10)	498 (20)	3633 (13)	166 (14)

[a] Equivalent isotropic *U* defined as one-third of the trace of the orthogonalized U_{ij} tensor.

mination and refinement, anisotropic thermal parameters, and hydrogen atom locations are available as supplementary material.

Experimental Results

Charge distribution within the tris(3,5-di-*tert*-butylquinone) complexes, $M(DBQ)_3$, containing metals of the second transition series appears to shift from $M^{VI}(DBCat)_3$ to $M^{III}(DBSQ)_3$ on moving from technetium to rhodium. The ruthenium complex has been synthesized by adding a solution containing the potassium salt of DBSQ, prepared by treating 3,5-di-*tert*-butylcatechol with base in air, to a $RuCl_3$ solution. Griffith has reported the synthesis of the osmium analogue, $Os(DBQ)_3$, by treating OsO_4 with 3,5-di-*tert*-butylcatechol in a reaction that involves both reduction of the metal and chelation by the catechol in a manner similar to the DBCat reactions with pertechnetate and perrhenate.[14,18] Full characterization of the ruthenium complex has been carried out to provide information on charge distribution in complexes close to the crossing point in Chart I. Additionally, stereochemical properties of both the ruthenium and osmium complexes have been investigated in solution by NMR spectroscopy.

Crystallographic Characterization on $Ru(DBQ)_3$ and $Os(DBQ)_3$. Two isomers exist for $Ru(DBQ)_3$ due to the asymmetry of the substituted catechol ligand. Structural characterizations on $Tc(DBCat)_3$, $Re(DBCat)_3$, $V(DBCat)_3^-$, $Cr(DBSQ)_3$, and $Fe(DBSQ)_3$ have all been carried out on crystals of the C_3-cis (facial) isomer.[3,10,11,14,15] The structure of $Os(DBQ)_3$, reported by Griffith and Hursthouse,[18a] was carried out on the C_1-trans (meridional) isomer. In this report we present structural characterization on both the cis and trans isomers of $Ru(DBQ)_3$ and on *trans*-$Os(DBQ)_3$ at −60 °C. Views of the two isomers of $Ru(DBQ)_3$ are shown in Figures 1 and 2; bond distances and angles for all three structure determinations are given in Table V. The octahedral complex molecules are distorted slightly toward a trigonal-prismatic inner coordination geometry by rotation of the triangular faces formed by oxygen atoms of the three ligands to give twist angles of 49°, 49°, and 48° for *trans*-$Ru(DBQ)_3$, *trans*-$Os(DBQ)_3$, and *cis*-$Ru(DBQ)_3$, respectively. Values of 0° and 60° would be expected for regular trigonal-prismatic and octahedral structures; intermediate values of 38° and 42° were found for the cis catecholate complexes $Re(DBCat)_3$ and $Tc(DBCat)_3$, and values of 38 and 49° were found for the cis semiquinone complexes $Fe(DBSQ)_3$ and $Cr(DBSQ)_3$.

Average Ru–O bond lengths for the two isomers of $Ru(DBQ)_3$ are relatively short, pointing to a high oxidation state for the metal. Values for *cis*-$Ru(DBQ)_3$ average to 1.976 (4) Å and range from 1.960 (3) to 1.988 (4) Å, while the average for *trans*-$Ru(DBQ)_3$ is 1.969 (10) Å with individual values ranging from 1.941 (10) to 1.997 (10) Å. A short Ru(IV)–O length of 1.974 (4) Å was reported for dichloro(triazene-1-oxidato)ruthenium(IV),[21] and the

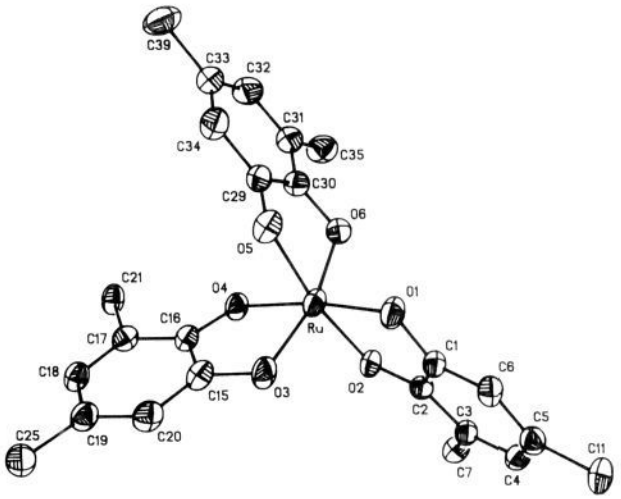

Figure 1. Plot showing the structure of *cis*-$Ru(DBQ)_3$.

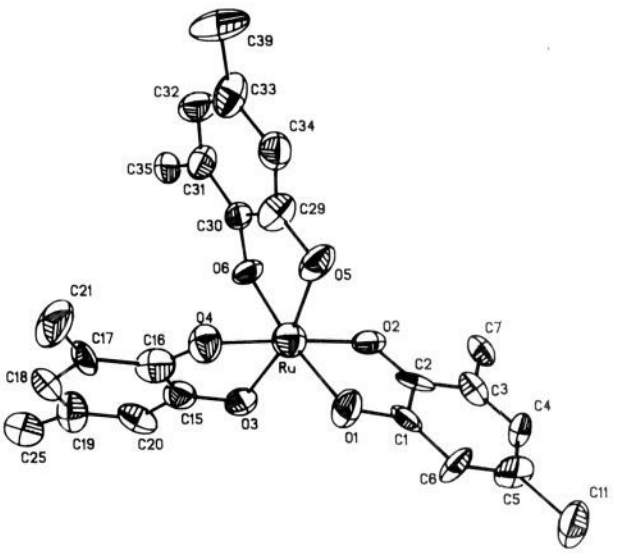

Figure 2. Plot showing the structure of *trans*-$Ru(DBQ)_3$.

DBQ complex Ru(*t*-Bupy)(DBQ)$_2$, where the C–O length for the quinone ligands was 1.322 (5) Å and metal charge was ambiguous, also has relatively short Ru–O lengths of 1.974 (4) Å.[19] The phenolato Ru(III)–O lengths of *mer*-Ru(sal)$_3$ average to 1.981 (2) Å,[22] but normal Ru–O lengths for Ru(III) are 2.00 Å or greater. Carbon–oxygen bond lengths for the quinone ligands often point to a specific ligand charge, semiquinonate or catecholate. The average C–O length of *cis*-Ru(DBQ)$_3$ is an intermediate value of 1.320 (6) Å. Large esd's limit the significance of the comparison for *trans*-Ru(DBQ)$_3$, but the values given in Table V and the average value of 1.30 (2) Å are more semiquinonate-like than catecholate. Two of the ligands have short and long C–O lengths similar to the semiquinonate ligand in Ru(bpy)$_2$(DBSQ)$^+$, with the shortest Ru–O lengths to the oxygens with the longest C–O lengths. Further, ring C–C bond lengths of ligands of both isomers show a consistent pattern with the shortest values for the C3–C4 and C5–C6 bonds of the 3,5-di-*tert*-butyl-1,2-benzoquinone-derived ligands. These bonds would be localized double bonds for the benzoquinone and are typically the shortest ring lengths of semiquinone ligands.[9]

Metal and ligand structural features fail to point to a clear charge distribution for the isomers of Ru(DBQ)$_3$. Average ligand C–O lengths are shorter than the 1.334 (13) Å value of Tc(DBCat)$_3$[14] but longer than the 1.281 (3) Å value of Fe(DBSQ)$_3$,[9] and the short Ru–O values suggest an oxidation state for the metal that is greater than Ru(III). Hursthouse and Griffith reported structural characterization on Os(Cat)$_3$ and *trans*-Os(DBCat)$_3$, and the results of these determinations also failed to provide information on charge distribution. While average Os–O lengths were found to be slightly shorter than the Ru–O values of the Ru(DBQ)$_3$ isomers and C–O values were slightly longer, both sets of lengths showed considerable variation as in *trans*-Ru(DBQ)$_3$. Os–O lengths ranged between 1.947 (6) and 1.985 (5) Å, and C–O values ranged between 1.30 (1) and 1.36 (1) Å. To reduce the effect of thermal distortion, a crystallographic data set was collected on a crystal of *trans*-Os(DBQ)$_3$ at −60 °C. Selected bond distances and angles are given in Table V, and the atom-numbering scheme used for *trans*-Os(DBQ)$_3$ is the same as that used for *trans*-Ru(DBQ)$_3$. In general, the average Os–O length of 1.958 (7) Å is 0.01 Å shorter than the Ru(DBQ)$_3$ value and agrees well with the room-temperature value of 1.958 (7) Å. Effective radii for high oxidation state ions of Ru are generally 0.01 Å shorter than corresponding values for osmium,[23] and the shorter Os–O lengths of Os(DBQ)$_3$ point to stronger bonding for the quinone ligands. While there is more consistency in the values for the C–O lengths for the −60 °C structure, the broad range of Os–O values found by Hursthouse and Griffith appears also at low temperature. In fact, for all three independent structure determinations on *trans*-Ru(DBQ)$_3$ and *trans*-Os(DBQ)$_3$, the pattern of short and long M–O lengths is the same, and this is also carried over to the pattern in C–O lengths where the longest values are found to oxygens O4 and O6. The average C–O length of 1.331 (13) Å for Os(DBQ)$_3$ is in agreement with the room-temperature value of 1.33 (1) Å and is slightly more catecholate-like than the average values found for the two Ru(DBQ)$_3$ isomers. Structural characterization on Os(bpy)$_2$(DBCat)$^+$ has also provided features for the quinone ligand that are more in accord with a catecholate formulation than the values found for the ruthenium analogue.[24] However, detailed features of Ru(DBQ)$_3$ and Os(DBQ)$_3$ are consistent with neither semiquinonate nor catecholate charge formulations for the ligands.

Spectroscopic Properties of Ru(DBQ)$_3$ and Os(DBQ)$_3$. Infrared spectra on Ru(DBQ)$_3$ and Os(DBQ)$_3$ are quite similar but differ from the spectra of Re(DBCat)$_3$ and Fe(DBSQ)$_3$ shown in Figure 3. In the region between 1000 and 1600 cm^{-1}, strong, broad, asymmetric envelopes of bands at 1155 (Ru) and 1158 cm^{-1} (Os) dominate the spectra. For Fe(DBSQ)$_3$, the dominant feature is a strong, asymmetric band at 1480 cm^{-1}, and the spectrum of Re(DBCat)$_3$ consists of strong, sharp bands at 1592, 1363, and 1200 cm^{-1}.

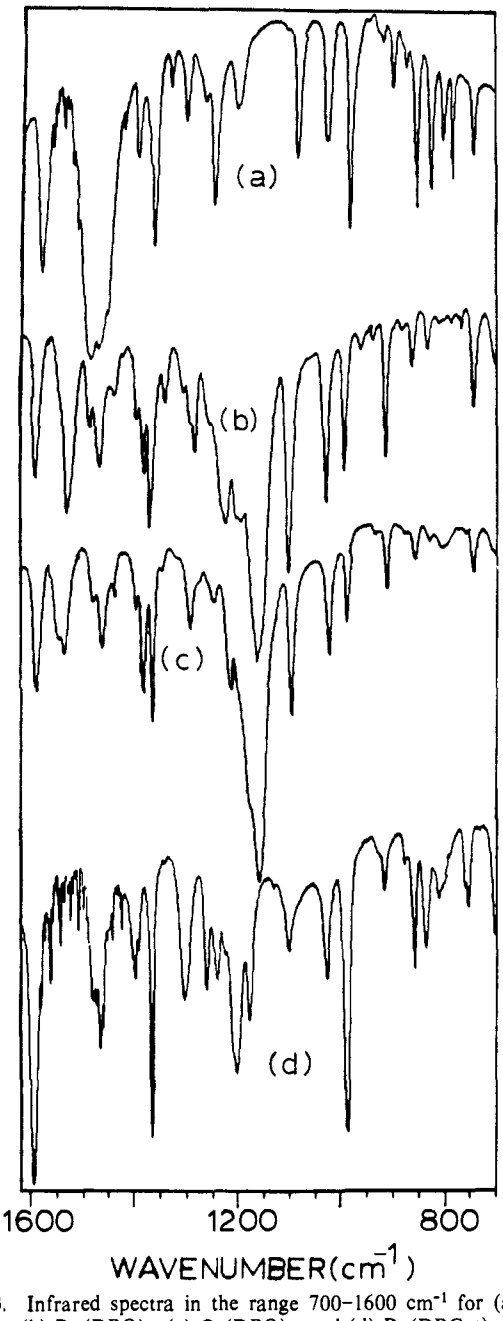

Figure 3. Infrared spectra in the range 700–1600 cm^{-1} for (a) Fe(DBSQ)$_3$, (b) Ru(DBQ)$_3$, (c) Os(DBQ)$_3$, and (d) Re(DBCat)$_3$.

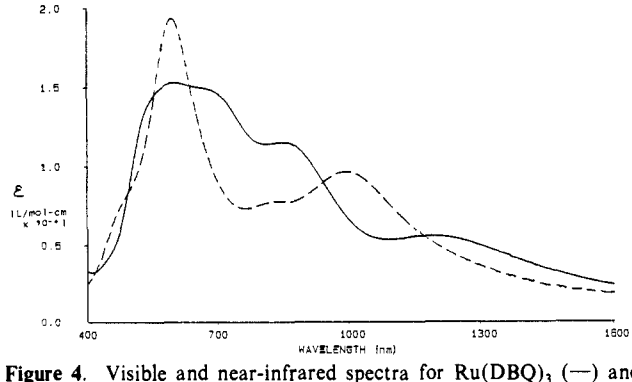

Figure 4. Visible and near-infrared spectra for Ru(DBQ)$_3$ (—) and Os(DBQ)$_3$ (---) recorded in CH_2Cl_2 solution.

(21) Bhattacharya, S.; Chakravorty, A.; Cotton, F. A.; Mukherjee, R.; Schwotzer, W. *Inorg. Chem.* **1984**, *23*, 1709.
(22) Bag, N.; Lahiri, G. K.; Bhattacharya, S.; Falvello, L. R.; Chakravorty, A. *Inorg. Chem.* **1988**, *27*, 4396.
(23) Shannon, R. D. *Acta Crystallogr., Sect. A: Cryst. Phys, Diffr., Theor. Gen. Crystallogr.* **1976**, *A32*, 751.
(24) Haga, M.; Boone, S. R.; Pierpont, C. G. Manuscript in preparation.

Table V. Selected Bond Distances (Å) and Angles (deg) for *cis*-Ru(DBQ)$_3$, *trans*-Ru(DBQ)$_3$, and *trans*-Os(DBQ)$_3$

	cis-Ru(DBQ)$_3$	*trans*-Ru(DBQ)$_3$	*trans*-Os(DBQ)$_3$
	Metal–Oxygen Lengths		
M–O1	1.983 (3)	1.997 (10)	1.984 (7)
M–O2	1.988 (4)	1.983 (8)	1.950 (7)
M–O3	1.960 (3)	1.976 (10)	1.963 (7)
M–O4	1.972 (3)	1.954 (9)	1.953 (7)
M–O5	1.978 (4)	1.961 (11)	1.951 (7)
M–O6	1.973 (4)	1.941 (10)	1.947 (7)
	Metal–Oxygen Angles		
O1–M–O2	80.0 (1)	79.0 (4)	78.9 (3)
O3–M–O4	81.1 (1)	81.7 (4)	80.7 (3)
O5–M–O6	81.7 (1)	83.2 (4)	81.1 (3)
O1–M–O3	89.0 (1)	98.9 (4)	98.7 (3)
O1–M–O4	170.0 (1)	99.3 (4)	99.2 (3)
O1–M–O5	96.3 (2)	92.5 (4)	92.9 (3)
O1–M–O6	105.4 (1)	172.5 (4)	171.9 (3)
O2–M–O4	99.6 (1)	176.5 (4)	174.6 (3)
O2–M–O5	170.5 (1)	96.2 (4)	96.8 (3)
O2–M–O6	90.0 (1)	95.4 (4)	96.2 (3)
O3–M–O5	91.9 (2)	164.9 (4)	165.1 (3)
O4–M–O5	85.6 (1)	86.8 (4)	88.3 (3)
O4–M–O6	84.6 (1)	86.6 (4)	86.2 (3)
	Ligand 1		
O1–C1	1.319 (6)	1.31 (2)	1.32 (1)
O2–C2	1.299 (5)	1.28 (2)	1.32 (1)
C1–C2	1.431 (7)	1.45 (2)	1.41 (1)
C2–C3	1.442 (7)	1.42 (2)	1.42 (1)
C3–C4	1.374 (6)	1.35 (2)	1.37 (1)
C4–C5	1.430 (8)	1.46 (2)	1.42 (1)
C5–C6	1.386 (7)	1.36 (2)	1.37 (1)
C1–C6	1.399 (6)	1.37 (2)	1.40 (1)
	Ligand 2		
O3–C15	1.326 (5)	1.29 (2)	1.32 (1)
O4–C16	1.320 (6)	1.33 (2)	1.35 (1)
C15–C16	1.417 (7)	1.44 (2)	1.39 (1)
C16–C17	1.409 (6)	1.42 (2)	1.41 (1)
C17–C18	1.387 (7)	1.37 (2)	1.37 (1)
C18–C19	1.421 (7)	1.45 (2)	1.45 (1)
C19–C20	1.369 (7)	1.38 (2)	1.38 (1)
C15–C20	1.403 (7)	1.39 (2)	1.41 (1)
	Ligand 3		
O5–C29	1.335 (6)	1.28 (2)	1.33 (1)
O6–C30	1.321 (6)	1.34 (2)	1.34 (1)
C29–C30	1.404 (8)	1.47 (2)	1.42 (1)
C30–C31	1.427 (7)	1.39 (2)	1.41 (1)
C31–C32	1.386 (8)	1.36 (2)	1.38 (1)
C32–C33	1.427 (9)	1.45 (2)	1.40 (1)
C33–C34	1.356 (8)	1.38 (2)	1.36 (1)
C29–C34	1.414 (8)	1.42 (2)	1.38 (1)

Electronic spectra for Ru(DBQ)$_3$ and Os(DBQ)$_3$ shown in Figure 4 consist of intense bands that extend into the near-infrared. Both complexes show two intense bands in the UV at 231 nm (ϵ 30 600 L cm^{-1} mol^{-1}) (Ru) and 232 nm (22 100) (Os), with shoulders that extend into the visible at 275 (16 400) and 353 nm (5000) for Ru(DBQ)$_3$ and at 286 (12 000) and 474 nm (7500) for Os(DBQ)$_3$. In the visible region, Ru(DBQ)$_3$ has two bands at 600 (16 400) and 690 nm (16 600), while Os(DBQ)$_3$ has a single band at 598 nm (19 500). Further into the near-infrared of Ru(DBQ)$_3$ has bands at 875 (9000) and 1250 nm (5500), and Os(DBQ)$_3$ has bands at 810 (7200) and 1000 nm (9500). Through the UV–vis, the spectra of the Ru and Os complexes are similar to the spectra of Tc(DBCat)$_3$ and Re(DBCat)$_3$. However, the Tc and Re complexes fail to show low-energy transitions in the near-infrared.

Electrochemistry on Ru(DBQ)$_3$ and Os(DBQ)$_3$. Dichloromethane solutions of Ru(DBQ)$_3$ and Os(DBQ)$_3$ have been investigated with cyclic voltammetry. Both complexes undergo two oxidation and two reduction reactions as shown for Os(DBQ)$_3$ in Figure 5. The reductions with coupled quasi-reversible oxidations occur at ΔE values of −0.52 (93) and −1.14 (99) V (vs Fc/Fc$^+$) for the ruthenium complex and −0.47 (96) and −1.24 (138) V for Os(DBQ)$_3$. As a general periodic trend, metal-based redox couples of third-row metals are shifted to negative potentials relative to corresponding couples of their second-row congeners.[25] Electrochemical characterization on complexes of the Mo/W and Tc/Re pairs has shown this to be the case for the tris(catecholate) complexes, where reduction must occur at the metal. The first reduction of Os(DBQ)$_3$ occurs at a slightly more positive potential than the corresponding reduction of Ru(DBQ)$_3$. As such, the first reduction step appears to be a ligand-based process or reduction of an electronic level that contains a strong ligand orbital component, indicating that the ligands of the two complexes remain partially oxidized relative to the ligands of the Mo/W and Tc/Re series.[14,26] The second reduction step conforms to the pattern expected of a metal-based reduction. Products of these reduction processes have as charge distributions M^{V}(DBCat)$_3^-$ and M^{IV}(DBCat)$_3^{2-}$ (M = Ru, Os). Oxidation couples for the two complexes occur at 0.35 (78) and 0.90 (147) V for Ru(DBQ)$_3$ and 0.52 (75) and 1.11 (162) V for Os(DBQ)$_3$. Both couples appear to be ligand-based. To investigate this possibility, Ru(DBQ)$_3$ was oxidized by addition of 1 equiv of Cu^{2+}/CH$_3$CN and the EPR spectrum of the resulting cation was studied. The first-derivative spectrum consists of a single resonance centered at a g value of 1.9993 with no resolvable hyperfine and a peak-to-peak separation of 8 G.

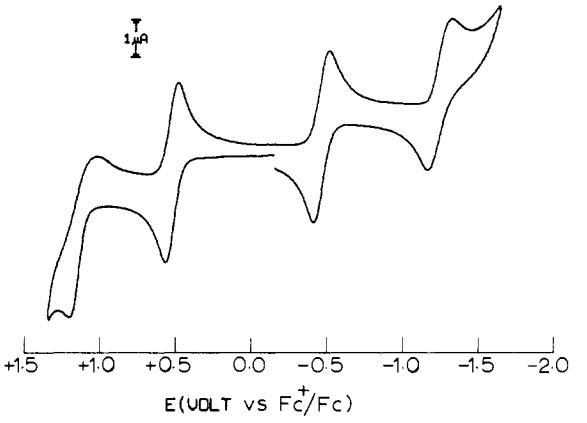

Figure 5. Cyclic voltammogram for Os(DBQ)$_3$ recorded in CH_2Cl_2 at a scan rate of 100 mV/s.

NMR Spectra of Ru(DBQ)$_3$ and Os(DBQ)$_3$. The neutral complexes M(DBQ)$_3$ (M = Ru) Os are both diamagnetic and exhibit sharp NMR resonances at room temperature. Spectra on Ru(DBQ)$_3$, recorded in CD_2Cl_2 solution at room temperature and shown in Figure 6, consist of eight singlet *tert*-butyl proton resonances at 1.267, 1.290, 1.296, 1.309, 1.326, 1.345 ppm, with two resonances overlapped at 1.332 ppm. Eight doublet phenyl proton resonances appear at 7.060, 7.236, 7.249, 7.272, 7.345, 7.363, 7.404, and 7.455 ppm, each split by 2.1-Hz coupling to the second ring proton. Intensity differences indicate the ring proton resonances at 7.404 and 7.249 ppm are associated with the C_3-cis isomer. The stereorigidity of this complex is in accord with the stereochemical properties of ruthenium(III) complexes containing β-diketonate and tropolonate ligands that show no evidence of exchange broadening in their NMR spectra up to temperatures of 170 °C.[27]

In marked contrast to this result, the osmium complex, Os(DBQ)$_3$, shows two sharp singlets in the *tert*-butyl region at 1.327 and 1.422 ppm and two doublet phenyl ring proton resonances at 6.682 and 7.476 ppm, each split by 2.1 Hz. This must result from isomerism that is rapid on the NMR time scale. To in-

(25) See for example: *Encyclopedia of Electrochemistry of the Elements*; Bard, A. J., Ed.; Marcel Dekker: New York, 1976; Vol. VI.

(26) DeLearie, L. A.; Haltiwanger, R. C.; Pierpont, C. G. *Inorg. Chem.* **1988**, *27*, 3842.

(27) (a) Fay, R. C.; Girgis, A. Y.; Klabunde, U. *J. Am. Chem. Soc.* **1970**, *92*, 7056. (b) Gordon, J. G., II; O'Connor, M. J.; Holm, R. H. *Inorg. Chim. Acta* **1971**, *5*, 381. (c) Eaton, S. S.; Eaton, G. R.; Holm, R. H.; Muetterties, E. L. *J. Am. Chem. Soc.* **1973**, *95*, 1116.

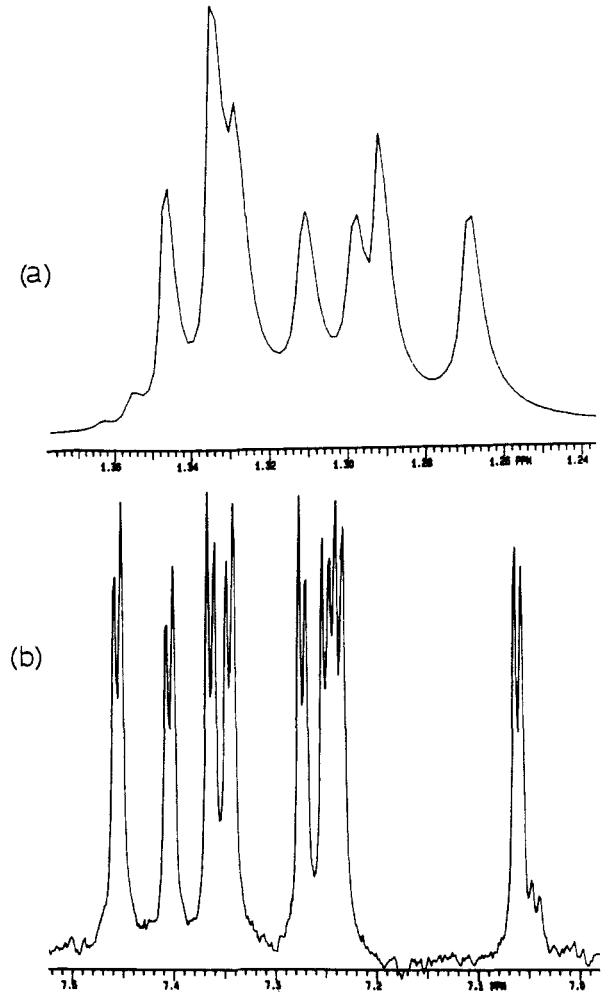

Figure 6. NMR spectrum of $Ru(DBQ)_3$ recorded at room temperature in CD_2Cl_2 showing the (a) *tert*-butyl and (b) ring proton regions of the spectrum.

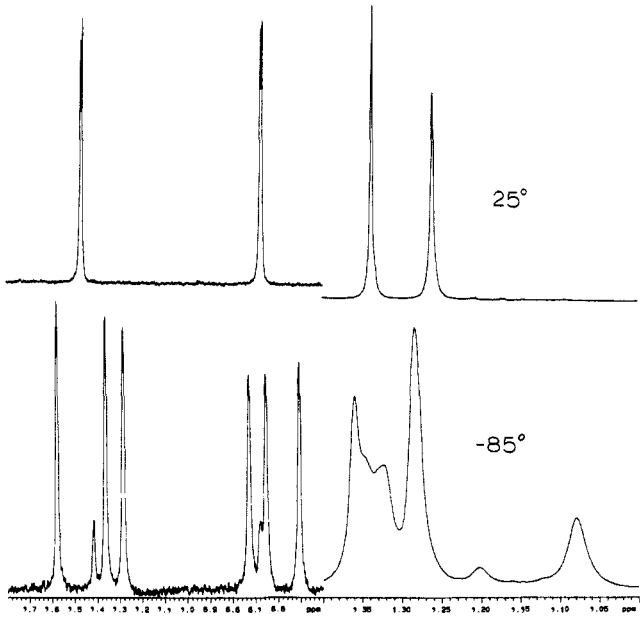

Figure 7. Limiting NMR spectra of $Os(DBQ)_3$ in the ring (left) and *tert*-butyl (right) proton regions recorded in CD_2Cl_2 solutions at 25 and −85 °C.

vestigate the dynamic properties of $Os(DBQ)_3$ in dichloromethane solution, 300-MHz NMR spectra were recorded on the complex at low temperature. Spectra obtained on the phenyl and *tert*-butyl proton regions are shown in Figure 7. At −85 °C, eight ring

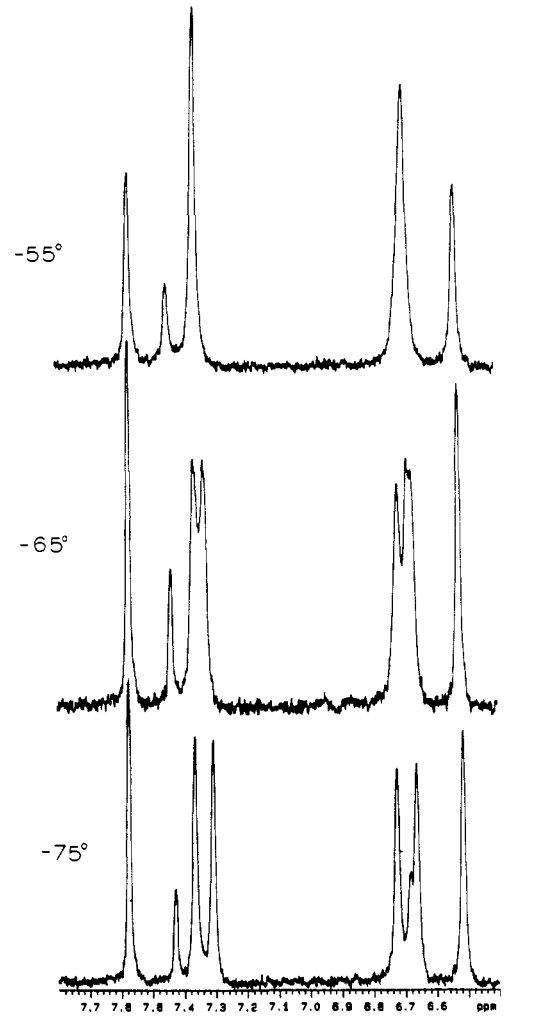

Figure 8. Coalescence of resonances for ring protons bonded to atoms C6 and C34 (Figure 2) of *trans*-$Os(DBQ)_3$ as the rate of racemization increases over the temperature range from −75 to −55 °C.

Scheme I

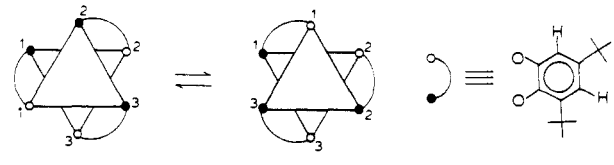

proton resonances appear quite clearly, and, while resolution is less clear, eight resonances also appear in the *tert*-butyl region. Two ring proton resonances at 7.42 and 6.69 ppm may be assigned to the C_3-cis isomer that is present in solution at this temperature at the equilibrated level of approximately 5%. One of the *tert*-butyl resonances of the cis isomer appears at 1.20 ppm; the other lies beneath the cluster of peaks in the 1.30–1.35 ppm region. Six sharp ring proton resonances appear for the nonequivalent ligands of the C_1-trans isomer, and from their behavior with increasing temperature, it is possible to make ligand assignments. Racemization of the trans isomer of a tris-chelated complex containing unsymmetrical ligands by a Bailar (trigonal) twist mechanism would interconvert two ligands, 2 and 3 in Scheme I, while the third remains unique. Referring to the numbering scheme given for the ruthenium molecule in Figure 2, protons on carbon atoms C4 and C32 and protons on C6 and C34 would be interconverted, while protons on C18 and C20 would remain unchanged. As the temperature of the solution is increased from −85 °C (Figure 8), resonances at 7.28 and 7.36 ppm coalesce as do resonances at 6.66 and 6.74 ppm. These correspond to the C4–C32 and C6–C34 sets of protons, although it is not possible to make specific assignments to the pairs. Resonances at 7.58 and 6.51 ppm remain discrete and can be assigned to the protons of carbons C18 and

Scheme II

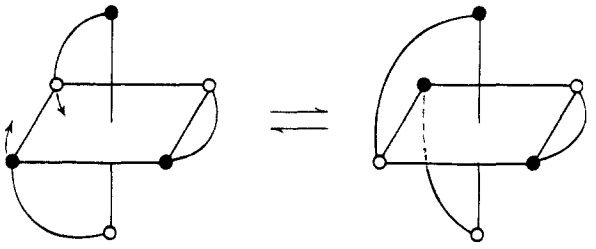

C20. A similar analysis of the *tert*-butyl resonances is more difficult. Resonances at 1.08 and 1.36 ppm appear not to be involved with a process leading to coalescence over this temperature range and may be assigned to the *tert*-butyl groups associated with carbons C21 and C25. Resonances at 1.32 and 1.34 ppm coalesce, and the broad resonance at 1.28 ppm appears to sharpen over this temperature range as *tert*-butyl groups associated with carbons C7 and C35 and C11 and C39 become equivalent with the increased rate of rearrangement. Full coalescence of proton resonances that would be related by a Bailar twist mechanism has occurred by −52 °C. These spectral changes have been simulated, and the values obtained for rate constants have been used to estimate the activation energy for the process at 12 kcal/mol.

At higher temperatures a second rearrangement process becomes operative: a process that isomerizes cis and trans forms of the complex. A dissociative process is unlikely due to the kinetic stability of high oxidation state metals of the second and third transition series. Further, there is no reason to expect that the osmium of $Os(DBQ)_3$ would be more labile than the ruthenium of $Ru(DBQ)_3$. This process begins to appear at temperatures slightly above the trans racemization coalescence temperature. Ring proton resonances associated with carbon atoms C18 and C20 and the ring proton resonances for the cis isomer coalesce with the C4–C32 and C6–C34 resonances to ultimately give two sharp resonances in the ring proton region as shown in Figure 9. The coalescence temperature for this process is approximately −18 °C, activation energy has been estimated to be 25 kcal/mol, and the isomerization process with a reasonable transition-state energy is the Ray–Dutt (rhombic) twist shown in Scheme II.

Mechanisms for isomerization and racemization in tris-chelated octahedral complexes have been of great interest as fundamental topics in inorganic stereochemistry.[28-31] Most recently, Rodger and Johnson analyzed nondissociative mechanisms in terms of transition-state energies.[29] The principal components in this analysis were M–L bond energy and L--L dispersion attraction. The Bailar twist and the Ray–Dutt twist were found to proceed through transition states of reasonable energy, each with trigonal-prismatic structures. Further differentiation between these two mechanisms could be made in terms of the L--L separation between donor atoms of a common ligand (*b*) and the interligand interdonor separation at a C_3 trigonal face of the octahedron (*l*). In cases where the *b*/*l* ratio is large, approximately 1.5, the Ray–Dutt transition state is lowest in energy. When the ratio is small, 0.5, the Bailar mechanism would be favored, and when the values are approximately equal, rearrangement may proceed by either mechanism. From the structural data on the isomers of $Ru(DBQ)_3$ and $Os(DBQ)_3$, *b*/*l* values of 0.90 and 0.89 are obtained, both close to the value of 0.91 at which transition-state energies for the two mechanisms are exactly equal in the Rodger–Johnson analysis. Factors related to electronic structure are difficult to include in such a model and are clearly significant in the present case. With the structural and spectral similarities found for the Ru and Os complexes, subtle electronic differences are responsible for the rigidity of the Ru complex and the fluxional character of the Os complex. Given the fluxional nature of the Os complex, structural features indicate that Bailar and Ray–Dutt transition states are similar in energy, with the Bailar mechanism slightly favored. The NMR properties of the complex are in accord with this expectation, and the difference in activation energies for the two processes is roughly 13 kcal/mol.

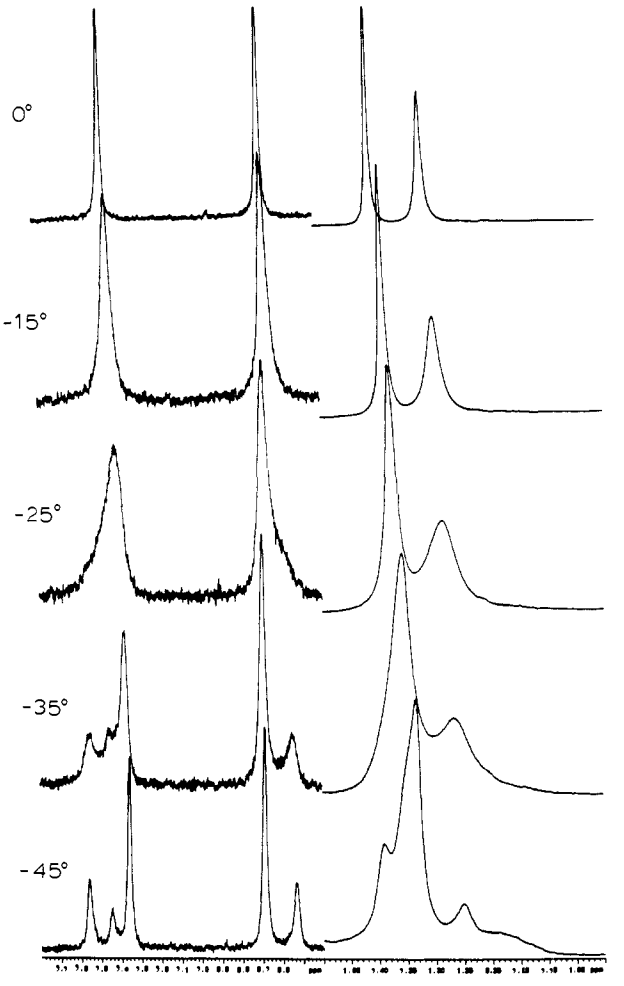

Figure 9. Coalescence of ring (left) and *tert*-butyl (right) proton resonances of *trans*-$Os(DBQ)_3$ as the rate of structural isomerization increases over the temperature range from −45 to 0 °C.

Charge Distribution in $Ru(DBQ)_3$ and $Os(DBQ)_3$. Periodic trends in charge distribution for semiquinone and catecholate complexes suggest that $Ru(DBQ)_3$ and $Os(DBQ)_3$ should have electronic structures that are intermediate between the $M^{VI}(DBCat)_3$ and $M^{III}(DBSQ)_3$ charge-localized limiting forms. Infrared spectra on the two complexes are similar but show clear differences from spectra obtained on semiquinone and catecholate complexes with more well-defined charge distributions. Structural features fail to point to specific charges for the metals and ligands, and both complexes show charge-transfer transitions in the near-infrared, as is typical of quinone complexes with metal and ligand electronic levels that are close in energy. In contrast to complexes of metals from groups on either side, the physical properties of $Ru(DBQ)_3$ and $Os(DBQ)_3$ reflect metal–ligand delocalization, and thermal population of low-lying excited-state electronic levels contributes to this electronic structure.

Further, differences in the solution stereochemical properties appear related to a subtle difference in metal charge between $Ru(DBQ)_3$ and $Os(DBQ)_3$. The ruthenium complex is rigid on the NMR time scale, a property shared by Ru(III) β-diketonate and tropolonate complexes, while $Os(DBQ)_3$ is fluxional. NMR spectra recorded on $Os(DBQ)_3$ over the temperature range between −85 and +25 °C show evidence for two intramolecular rearrangement processes: racemization at low temperatures and isomerization as a process with slightly higher activation energy. Dithiocarbamate complexes of Ru and Os have been observed to undergo optical inversion in solution, and the rate of inversion for

(28) Eaton, S. S.; Hutchison, J. R.; Holm, R. H.; Muetterties, E. L. *J. Am. Chem. Soc.* **1972**, *94*, 6411.
(29) Rodger, A.; Johnson, B. F. G. *Inorg. Chem.* **1988**, *27*, 3061.
(30) Muetterties, E. L. *J. Am. Chem. Soc.* **1968**, *90*, 5097.
(31) Keppert, D. L. *Prog. Inorg. Chem.* **1977**, *23*, 1.

$Os(Et_2dtc)_3$ was found to be slightly greater than that of $Ru(Et_2dtc)_3$.[32] The difference in the stereodynamic properties between $Ru(DBQ)_3$ and $Os(DBQ)_3$ is more dramatic, however. Similarities in b/l ratio and twist angle, structural features that should be sensitive to transition-state energy for intramolecular rearrangement, indicate that the difference in fluxional character results from a ligand field effect. Even though infrared spectra fail to detect a difference in electronic structure, the M–O and C–O lengths obtained from the four structure determinations point to a higher charge for the metal of $Os(DBQ)_3$. While there is a clear difference in electron distribution for metals of adjacent groups, there appears to also be a difference in metal charge for the three members of the iron triad.

(32) Given, K. W.; Wheeler, S. H.; Jick, B. S.; Maheu, L. J.; Pignolet, L. H. *Inorg. Chem.* **1979**, *18*, 1261.

Acknowledgment. This research was supported by the National Science Foundation under Grant CHE 88-09923 and by the Army Research Office under Grant DAAL 03-88-K-0130. We thank Martin Ashley for patient instruction on use of the NMR, Dr. Linda Luck for help with simulation of NMR spectra, and Dr. Subhash Padhye for help with initial stages of synthesis on $Ru(DBQ)_3$.

Supplementary Material Available: Tables containing details of the structure determinations on *cis*-$Ru(DBQ)_3$, *trans*-$Ru(DBQ)_3$, and *trans*-$Os(DBQ)_3$, anisotropic thermal parameters for the atoms of all three structures, complete lists of bond distances and angles, and hydrogen atom locations (27 pages). Ordering information is given on any current masthead page.

Alkylnickel and -palladium Alkoxides Associated with Alcohols through Hydrogen Bonding

Yong-Joo Kim,[1] Kohtaro Osakada,*[1] Akio Takenaka,[2] and Akio Yamamoto*[1]

Contribution from the Research Laboratory of Resources Utilization, Tokyo Institute of Technology, and Department of Life Science, Faculty of Science, Tokyo Institute of Technology, 4259 Nagatsuta, Midori-ku Yokohama 227, Japan. *Received April 26, 1989*

Abstract: *trans*-PdR_2L_2 (R = CH_3, C_2H_5; L = PMe_3, PEt_3) and *trans*-$NiMe_2(PMe_3)_2$ react with 2 equiv of fluorinated alcohols and para-substituted phenols to give complexes formulated as *trans*-$PdR(OR')(HOR')L_2$ (R' = $CH(CF_3)Ph$, C_6H_5, *p*-$CH_3C_6H_4$, *p*-$CH_3OC_6H_4$, *p*-ClC_6H_4, *p*-BrC_6H_4, *p*-FC_6H_4) and *trans*-$NiMe(OR')(HOR')(PMe_3)_2$ (R' = $CH(CF_3)Ph$, C_6H_5), respectively. IR and NMR spectra of these complexes indicate the presence of strong O–H···O hydrogen bonding between the alkoxide (or aryloxide) ligand and the alcohol (or substituted and nonsubstituted phenol) both in the solid state and in solution. X-ray crystallography of *trans*-$PdMe(OPh)(HOPh)(PMe_3)_2$ and *trans*-$NiMe(OPh)(HOPh)(PMe_3)_2$ shows that the phenoxide oxygen in each complex is associated with phenol through hydrogen bonding. Reactions of *trans*-$PdMe_2(PMe_3)_2$ with equimolar substituted and nonsubstituted phenols, respectively, give *trans*-$PdMe(OC_6H_4$-*p*-$X)(PMe_3)_2$ (X = H, Me, OMe, F, Cl, Br), which react with additional equimolar phenols to give phenol-bonded palladium complexes *trans*-$PdMe(OC_6H_4$-*p*-$X)(HOC_6H_4$-*p*-$X)(PMe_3)_2$. *trans*-$PdMe(OPh)(PMe_3)_2$ reacts also with fluorinated alcohols to give *trans*-$PdMe(OPh)(HOCH(CF_3)Ph)(PMe_3)_2$ and *trans*-$PdMe(OPh)(HOCH(CF_3)_2)(PMe_3)_2$, which are fully characterized by means of IR and NMR spectroscopy and X-ray crystallography. ^1H NMR spectra of mixtures of phenol with *cis*-$PdMe_2$(dmpe) (dmpe = 1,2-bis(dimethylphosphino)ethane) and *cis*-$PdMe_2$(dpe) (dpe = 1,2-bis(diphenylphosphino)ethane) indicate formation of strong O–H···O hydrogen bonding between phenol and the phenoxide ligand in solution. Equilibrium constants for the association of phenol with the palladium phenoxide having dmpe ligand, obtained by means of ^1H NMR spectroscopy, are smaller than those of *trans*-$PdMe(OPh)(PMe_3)_2$ with phenol. NMR spectra of *trans*-$PdMe(OCH(CF_3)Ph)(HOCH(CF_3)Ph)(PMe_3)_2$ and *trans*-$PdMe(OAr)(HOAr)(PMe_3)_2$ at variable temperatures (−60 to +40 °C) indicate the presence of intramolecular alkoxide-exchange process between the alkoxide ligand and the alcohol moiety on the NMR time scale. Addition of phenol to *trans*-$PdMe(OCH(CF_3)Ph)(HOCH(CF_3)Ph)(PMe_3)_2$ causes displacement of the alkoxide ligand by phenoxide group to give *trans*-$PdMe(OPh)(HOCH(CF_3)Ph)(PMe_3)_2$. Reactions of *trans*-$PdMe(OCH(CF_3)Ph)(HOCH(CF_3)Ph)(PMe_3)_2$ and *trans*-$PdMe(OPh)(HOCH(CF_3)Ph)(PMe_3)_2$ with CO give $MeCOOCH(CF_3)Ph$ in 99% and 46% yields, respectively. Reactions of *trans*-$PdMe(OCH(CF_3)Ph)(HOCH(CF_3)Ph)(PMe_3)_2$ with aryl esters give methylpalladium aryloxide complexes and esters of the fluorinated alcohol through exchange of the alkoxide group between the complex and the ester. The alkoxide (phenoxide) complexes catalyze transesterification of alcohols with esters. Mechanistic implications of the present results regarding the transesterification are presented.

Late-transition-metal alkoxides[3-11] are regarded as important intermediates in various transition-metal-catalyzed synthetic organic reactions. Those of platinum and iridium have recently attracted considerable attention. Chemical properties of these metal alkoxides regarding β-hydrogen elimination of the alkoxide

(1) Research Laboratory of Resources Utilization.
(2) Department of Life Science, Faculty of Science.
(3) (a) Bennett, M. A.; Robertson, G. B.; Whimp, P. O.; Yoshida, T. *J. Am. Chem. Soc.* **1973**, *95*, 3028. (b) Bennett, M. A.; Yoshida, T. *Ibid.* **1978**, *100*, 1750.
(4) Lehmkuhl, H.; Eisenbach, W. *Ann.* **1975**, 672.
(5) Yoshida, T.; Okano, T.; Otsuka, S. *J. Chem. Soc., Dalton Trans.* **1976**, 993.
(6) Michelin, R. A.; Napoli, M.; Ros, R. *J. Organomet. Chem.* **1979**, *175*, 239.
(7) (a) Komiya, S.; Tane-ichi, S.; Yamamoto, A.; Yamamoto, T. *Bull. Chem. Soc. Jpn.* **1980**, *53*, 673. (b) Hayashi, Y.; Komiya, S.; Yamamoto, T.; Yamamoto, A. *Chem. Lett.* **1984**, 1363.
(8) (a) Arthur, T.; Robertson, D. R.; Tocher, D. A.; Stephenson, T. A. *J. Organomet. Chem.* **1981**, *208*, 389. (b) Gould, R. O.; Stephenson, T. A.; Tocher, D. A. *J. Organomet. Chem.* **1984**, *263*, 375.
(9) (a) Bryndza, H. E.; Calabrese, J. C.; Wreford, S. S. *Organometallics* **1984**, *3*, 1603. (b) Bryndza, H. E.; Kretchmar, S. A.; Tulip, T. H. *J. Chem. Soc., Chem. Commun.* **1985**, 977. (c) Bryndza, H. E. *Organometallics* **1985**, *4*, 1686. (d) Bryndza, H. E.; Calabrese, J. C.; Marsi, M.; Roe, D. C.; Tam, W.; Bercaw, J. E. *J. Am. Chem. Soc.* **1986**, *108*, 4805.
(10) (a) Oro, L. A.; Carmona, D.; Lamata, M. P.; Apreda, M. C.; Foces-Foces, C.; Cano, F. A.; Maitlis, P. M. *J. Chem. Soc., Dalton Trans.* **1984**, 1823. (b) Lehoz, F. J.; Oro, L. A.; Lamata, M. P.; Puebla, M. P.; Foces-Foces, C.; Cano, F. A. *J. Organomet. Chem.* **1986**, *316*, 221.
(11) (a) Rees, W. M.; Churchill, M. R.; Fettinger, J. C.; Atwood, J. D. *Organometallics* **1985**, *4*, 2179. (b) Bernard, K. A.; Rees, W. M.; Atwood, J. D. *Ibid.* **1986**, *5*, 390. (c) Bernard, K. A.; Atwood, J. D. *Ibid.* **1987**, *6*, 1133. (d) Rappoli, B. J.; Janik, T. S.; Churchill, M. R.; Thomson, J. S.; Atwood, J. D. *Organometallics* **1988**, *7*, 1939.

0002-7863/90/1512-1096$02.50/0